

# *Fermi*-LAT Detection of a Break in the Gamma-Ray Spectrum of the Supernova Remnant Cassiopeia A

Y. Yuan<sup>1,2</sup>, S. Funk<sup>1,3</sup>, G. Jóhannesson<sup>4</sup>, J. Lande<sup>1,5</sup>, L. Tibaldo<sup>1</sup>, Y. Uchiyama<sup>6,7</sup>

## ABSTRACT

We report on observations of the supernova remnant Cassiopeia A in the energy range from 100 MeV to 100 GeV using 44 months of observations from the Large Area Telescope on board the *Fermi Gamma-ray Space Telescope*. We perform a detailed spectral analysis of this source and report on a low-energy break in the spectrum at  $1.72_{-0.89}^{+1.35}$  GeV. By comparing the results with models for the  $\gamma$ -ray emission, we find that hadronic emission is preferred for the GeV energy range.

*Subject headings:* gamma-rays: general, ISM: supernova remnants, supernovae: individual (Cassiopeia A), Acceleration of particles, radiation mechanisms: non-thermal

## 1. Introduction

With an age of  $\sim 350$  years, the supernova remnant (SNR) Cassiopeia A (Cas A) is one of the youngest objects of this class in our Galaxy. It is also one of the best studied objects with both thermal and non-thermal broad-band emission ranging from radio through X-ray all the way to GeV and TeV gamma rays. It is the brightest radio source in the sky outside

---

<sup>1</sup>W. W. Hansen Experimental Physics Laboratory, Kavli Institute for Particle Astrophysics and Cosmology, Department of Physics and SLAC National Accelerator Laboratory, Stanford University, Stanford, CA 94305, USA

<sup>2</sup>email: yuanyj@stanford.edu

<sup>3</sup>email: funk@slac.stanford.edu

<sup>4</sup>Science Institute, University of Iceland, IS-107 Reykjavik, Iceland

<sup>5</sup>email: joshualande@gmail.com

<sup>6</sup>3-34-1 Nishi-Ikebukuro, Toshima-ku, Tokyo, Japan 171-8501

<sup>7</sup>email: uchiyama@slac.stanford.edu

14 of our solar system (Baars et al. 1977) and is located at a distance of  $3.4_{-0.1}^{+0.3}$  kpc (Reed et al.  
 15 1995). Non-thermal emission tracing the acceleration of particles to relativistic energies  
 16 has been detected in both the forward and reverse shocks (see e.g. Gotthelf et al. 2001;  
 17 Hughes et al. 2000; Helder & Vink 2008; Maeda et al. 2009), in particular seen through high-  
 18 angular resolution X-ray studies. Fast variability and small filaments seen in these X-ray  
 19 observations also suggest rather large magnetic fields of 0.1-0.3 mG in the shock region of Cas  
 20 A (Patnaude & Fesen 2007, 2009; Uchiyama & Aharonian 2008). The observed brightness  
 21 variations might, however, also be produced by local enhancements of the turbulent magnetic  
 22 field (Bykov et al. 2008).

23 Gamma-ray observations further corroborate the existence of non-thermal particles in  
 24 the shell of Cas A. The SNR was first detected at TeV energies with the HEGRA telescope  
 25 system (Aharonian et al. 2001), later confirmed by MAGIC (Albert et al. 2007) and VERI-  
 26 TAS (Acciari et al. 2010), and subsequently detected at lower (GeV) energies with the Large  
 27 Area Telescope (LAT) on board the *Fermi Gamma-ray Space Telescope (Fermi)* (Paper I,  
 28 Abdo et al. 2010a). Those observations revealed a rather modest gamma-ray flux, compared  
 29 to the synchrotron radio through X-ray emission, further strengthening the argument for a  
 30 rather high magnetic field. The field can hardly be significantly less than  $100 \mu\text{G}$  (Abdo et al.  
 31 2010a), consistent with earlier studies (see e.g. Vink & Laming 2003; Parizot et al. 2006). It  
 32 should be stressed that the magnetic field is likely to be non-uniform. This was originally  
 33 proposed by Atoyan et al. (2000) who suggested greatly amplified magnetic fields of up to 1  
 34 mG in compact filaments. Because both the photon and matter densities in the shock regions  
 35 are rather high, these gamma-ray studies also suggested that the non-thermal electron (and  
 36 proton) densities are somewhat low, compared to estimates of the explosion energy (only a  
 37 few percent). The centroids for the GeV to TeV emission seem to be shifted towards the west-  
 38 ern region of the remnant where nonthermal X-ray emission is also brightest (Helder & Vink  
 39 2008; Maeda et al. 2009; Abdo et al. 2010a).

40 However, given the gamma-ray data published so far it was not possible to unam-  
 41 biguously determine the particle population responsible for the bulk of the emission, in  
 42 particular to distinguish between gamma rays produced through the bremsstrahlung and in-  
 43 verse Compton (IC) leptonic processes and the neutral pion decay hadronic process. Lower-  
 44 energy gamma rays (below 1 GeV) hold the key to distinguishing between these scenarios,  
 45 since a sharp low-energy roll-over in the spectrum of hadronically-produced gamma rays  
 46 is expected (Stecker 1971). Continuous observations of Cas A with the *Fermi*-LAT have  
 47 provided us a better opportunity to investigate the gamma-ray emission in the  $\lesssim 1$  GeV  
 48 range.

49 The LAT is a pair-conversion detector that operates between 20 MeV and  $> 300$  GeV.

50 The telescope has been in routine scientific operation since 2008 August 4. With its wide  
51 field of view of 2.4 sr, the LAT observes the whole sky every  $\sim 3$  hours. More details about  
52 the LAT instrument and its operation can be found in Atwood et al. (2009). In addition,  
53 the data reduction process and instrument response functions recently have been improved  
54 based on two years of in-flight data (so-called Pass7v6, Ackermann et al. 2012b). According  
55 to the updated instrument performance, the point-spread function of the LAT gives a 68%  
56 containment angle of  $< 6^\circ$  radius at 100 MeV and  $< 0.3$  at  $> 10$  GeV for normal incidence  
57 photons in P7SOURCE class. The sensitivity of the LAT for a point source with a power  
58 law photon spectrum of index 2 and a location similar to Cas A is  $\sim 9 \times 10^{-9}$  ph cm $^{-2}$ s $^{-1}$  for  
59 a  $5\sigma$  detection above 100 MeV after 44 months of sky survey. Our analysis takes advantage  
60 of both the increase in data quantity and quality.

61 In this letter, we describe our analysis method in § 2, present the *Fermi* results in § 3,  
62 and then discuss the gamma-ray emission mechanism of Cas A in § 4.

## 63 2. Analysis Method

64 We analyzed *Fermi*-LAT observations of Cas A using data collected from 2008 August  
65 4 to 2012 April 18 (Mission elapsed time 239557565.63 – 356436692.23, about 44 months of  
66 data). The analysis was performed in the energy range 100 MeV-100 GeV using the LAT Sci-  
67 ence Tools<sup>1</sup> as well as an independent tool `pointlike`. In particular, we used the maximum-  
68 likelihood fitting packages `pointlike` to fit the position and test for significant spatial exten-  
69 sion of Cas A, then with the updated localization result we used `gtlike` to fit the spectrum  
70 of the source. Our analysis procedure is very similar to that of the second LAT source cat-  
71 alog (2FGL, Nolan et al. 2012). When analyzing the data, we used the P7SOURCE class  
72 event selection and P7\_V6 instrument response functions (IRFs, Ackermann et al. 2012b).  
73 In order to reduce contamination from gamma rays produced in the Earth’s limb, we ex-  
74 cluded events with reconstructed zenith angle greater than  $100^\circ$ , and selected times when  
75 the rocking angle was less than  $52^\circ$ .

76 Emission produced by the interactions of cosmic rays with interstellar gas and radiation  
77 fields substantially contributes to the gamma-ray intensities measured by the LAT near the  
78 Galactic plane. We accounted for it using the standard diffuse model used in the 2FGL  
79 analysis. We also included the standard isotropic template accounting for the isotropic

---

<sup>1</sup>The LAT Science Tools are distributed through the *Fermi* Science Support Center (FSSC, <http://fermi.gsfc.nasa.gov>).

80 gamma-ray background and residual cosmic-ray contamination.<sup>2</sup> In addition, we modeled  
 81 as background sources all nearby 2FGL sources: in `pointlike` we used a circular region of  
 82 interest (ROI) with a radius of  $15^\circ$  centered on Cas A; in `gtlike` we used a square region of  
 83 interest with a size of  $20^\circ \times 20^\circ$  aligned with Galactic coordinates, using a spatial binning of  
 84  $0^\circ.125 \times 0^\circ.125$ . We adopt the same parameterizations as 2FGL for these sources, while left  
 85 free the spectral parameters of 5 2FGL sources that were either nearby or had a significant  
 86 residual when assuming the 2FGL values: 2FGL J2333.3+6237, 2FGL J2257.5+6222c, 2FGL  
 87 J2239.8+5825, 2FGL J2238.4+5902, 2FGL J2229.0+6114. In addition, we added 4 sources  
 88 not included in 2FGL which will be described in Section § 3.1.

### 89 3. Results

#### 90 3.1. Spatial Analysis

91 Because of the wide and energy-dependent point-spread function of the LAT, nearby  
 92 sources must be carefully modeled to avoid bias during a spectral analysis. Therefore, before  
 93 analyzing Cas A, we performed a dedicated search for nearby point-like sources not included  
 94 in the 2FGL catalog. We did so by adding sources in the background model at the positions of  
 95 significant residual test statistic (TS, which follows the same definition as that in Nolan et al.  
 96 2012) until the residual  $TS < 25$  within the entire `pointlike` ROI. Table 1 lists the four  
 97 significant new sources found in this study. We have not found any counterparts for the new  
 98 sources yet.

99 Figure 1 shows a count map above 800 MeV of the region surrounding Cas A. The  
 100 relatively bright source coincident with the SNR Cas A has a TS value of  $\sim 600$ . First, we  
 101 used `pointlike` to fit the position of this source and test for any possible spatial extension.  
 102 The best fit position of the source, in Galactic coordinates, is  $l, b = 111^\circ.74, -2^\circ.12$ , with a  
 103 statistical uncertainty of  $0^\circ.01$  (68% containment). To account for the systematic error in  
 104 the position of Cas A, we added  $0^\circ.005$  in quadrature as was adopted for the 2FGL analysis  
 105 (Nolan et al. 2012).

106 This location is only  $0^\circ.02$  away from the central compact object (CCO) (Pavlov & Luna  
 107 2009), as shown in Figure 2. This confirms that the GeV source is most likely the  $\gamma$ -ray  
 108 counterpart of the Cas A SNR. Following the method described in Lande et al. (2012), we  
 109 used a disk spatial model to fit the extension of Cas A. We found that the emission was not

---

<sup>2</sup>The diffuse model `gal_2yearp7v6_v0.fits` and isotropic template `isotrop_2year_P76_source_v0.txt` can be obtained through the FSSC.

110 significantly spatially extended ( $\text{TS}_{\text{ext}} = 0.1$ ) and has an extension upper limit of 0.1 at  
 111 95% confidence level. Note that this upper limit is larger than the shell of Cas A.

### 112 3.2. Spectral Analysis

113 We performed a spectral analysis of Cas A in the energy range from 100 MeV to 100 GeV  
 114 using `gtlike`. We first fit Cas A with a power-law spectral model and found an integral flux  
 115 of  $(6.17 \pm 0.43_{\text{stat}}) \times 10^{-11}$  erg cm $^{-2}$ s $^{-1}$  in the energy range from 100 MeV to 100 GeV and  
 116 a photon index of  $\Gamma = 1.80 \pm 0.04_{\text{stat}}$ . The results are consistent with the previous analysis  
 117 of Abdo et al. (2010a).

We then tested for a break in the spectrum of Cas A by fitting the spectrum with a smoothly-broken power-law spectral model

$$\frac{dN}{dE} = N_0 \left( \frac{E}{E_0} \right)^{-\Gamma_1} \left( 1 + \left( \frac{E}{E_b} \right)^{\frac{\Gamma_2 - \Gamma_1}{\beta}} \right)^{-\beta}. \quad (1)$$

118 Here,  $N_0$  is the prefactor;  $E_0$  is a fixed energy scale (taken to be 1 GeV);  $E_b$  is the break  
 119 energy;  $\Gamma_1$  and  $\Gamma_2$  are the photon indices before and after the break, respectively;  $\beta$  is a  
 120 small, fixed parameter that describes the smoothness of the transition at the break (taken  
 121 to be 0.1).

We tested for the significance of this spectral feature using a likelihood ratio test:

$$\text{TS}_{\text{break}} = 2 \log(\mathcal{L}_{\text{SBPL}}/\mathcal{L}_{\text{PL}}) \quad (2)$$

122 where  $\mathcal{L}$  is the Poisson likelihood of observing the given data assuming the best-fit model.  
 123 We obtained  $\text{TS}_{\text{break}} = 48.2$ , indicating that the break is significant. The resulting spectral  
 124 parameters are quoted in Table 2.

125 We then computed a spectral energy distribution (SED) in 8 bins per energy decade by  
 126 fitting the flux of Cas A independently in each energy bin (the lowest 6 bins were combined  
 127 into 3 bins). The SED of Cas A, along with the all-energy spectral fit, is plotted in Figure 3.  
 128 Statistical upper limits are shown in energy bins where TS of the flux is less than 4. These  
 129 upper limits are calculated at 95% confidence level using a Bayesian method (e.g., Helene  
 130 1983).

### 3.3. Systematic Errors

131

132 We estimated the systematic errors on the spectrum of Cas A due to uncertainty in our  
 133 model of the Galactic diffuse emission and due to uncertainty in our knowledge of the IRFs  
 134 of the LAT.

135 To probe the uncertainties due to the modeling of Galactic diffuse emission we use a se-  
 136 ries of alternative models (de Palma et al. 2013). These models differ from the standard one  
 137 in the sense that de Palma et al. 1) adopt different gamma-ray emissivities for the interstellar  
 138 gas, different gas column densities, and use a different approach for incorporating spatially  
 139 extended residuals; 2) vary a select number of important input parameters of the model  
 140 (Ackermann et al. 2012a): the H I spin temperature, the cosmic-ray source distribution, and  
 141 height of the cosmic-ray propagation halo; 3) allow more freedom in the fit by separately  
 142 scaling components of the model in four Galactocentric rings. Although these models do  
 143 not span the complete uncertainty of the systematics involved with Galactic diffuse emission  
 144 modeling, they were selected to probe the most important systematic uncertainties.

145 At low energy ( $< 1$  GeV), our uncertainty in the modeling of the Galactic diffuse emis-  
 146 sion leads to significant uncertainty in the spectral analysis of Cas A, because the integrated  
 147 intensity of the diffuse emission on the scale of the energy dependent point spread function  
 148 of the LAT becomes comparable with the flux of the source. By examining the residual  
 149 maps after fitting, we found that the standard diffuse model overshoots the data for a region  
 150  $\sim 2^\circ$  from Cas A (Figure 4), and this can lead to underestimated upper limits in the SED  
 151 calculation.

152 This overestimation of diffuse count is most likely due to uncertainty in modeling the  
 153 gamma-ray emission from the molecular complex associated with NGC 7538 and Cas A in the  
 154 Perseus arm (e.g., Abdo et al. 2010b). The alternative diffuse models provide a qualitatively  
 155 better fit of this region when the normalization of each Galactocentric ring was left free, since  
 156 the increased degrees of freedom allow us to better scale the Galactic diffuse model for this  
 157 specific region. The improvement can be seen in Figure 4 which shows a residual map with  
 158 the standard diffuse model and an improved residual map with one of the alternative diffuse  
 159 models.

160 Even though there is significant systematic uncertainty in the spectral model of Cas A  
 161 at lower energies,  $TS_{\text{break}}$  was greater than 20 using all of the alternative diffuse models and  
 162 is therefore robust against this systematic uncertainty.

163 We estimated the systematic error due to uncertainty in the IRFs using the method  
 164 described in Ackermann et al. (2012b). Following this method, we set the pivot in the  
 165 bracketing IRFs at 2 GeV, near the spectral peak in our SED. Again, we found the spectral

166 break to be robust against uncertainty in IRFs.

167 The systematic errors on the estimated spectral parameters due to both systematic  
 168 uncertainties are included in Table 2.

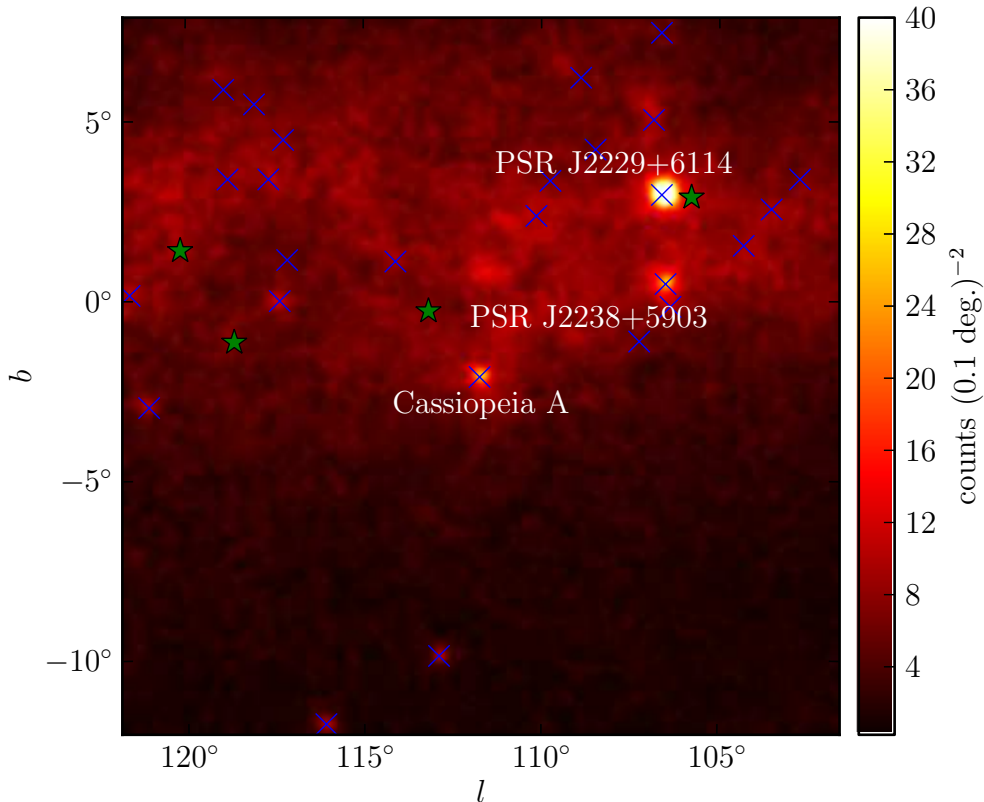


Fig. 1.— *Fermi*-LAT count map of the region surrounding Cas A ( $20^\circ \times 20^\circ$ ) from 800 MeV to 100 GeV. This plot is smoothed by a Gaussian kernel of size  $0.1$ . Also shown are the 2FGL sources included in our background model (blue crosses) and the new sources we added in (green stars).

169

#### 4. Discussion

170 In Figure 3, the new spectral data points measured with the *Fermi*-LAT are overlaid  
 171 with those from Paper I. The newly-measured spectrum is consistent with the previous  
 172 result, except that most of the new data points lie slightly above the old measurement. This  
 173 is likely due to the changed event classifications and improved IRFs of the LAT as well as



Table 1. New sources added to the ROI

Name	TS	$l$ (deg.)	$b$ (deg.)	Flux ( $10^{-8}$ ph cm $^{-2}$ s $^{-1}$ )	Index
Source 1	35.0	120.10	1.41	$1.96 \pm 0.53$	$2.24 \pm 0.10$
Source 2	31.7	118.59	-1.14	$0.89 \pm 0.40$	$2.04 \pm 0.15$
Source 3	25.6	113.16	-0.28	$0.66 \pm 0.31$	$1.92 \pm 0.16$
Source 4	24.8	105.82	2.89	$1.39 \pm 0.65$	$2.12 \pm 0.14$

Note. — The spectral and spatial parameters of the new sources found in the region surrounding Cas A.  $l$  and  $b$  are the Galactic longitude and latitude of the source and TS is the significance of the detection of the source (in the energy range from 100 MeV to 100 GeV). The sources were modeled with a power-law spectral model and the flux is computed from 100 MeV to 100 GeV.

Table 2. Spectral Results for Cas A

Parameters	Value	$\Delta_{\text{stat}}$	$\Delta_{\text{sys,diffuse}}$	$\Delta_{\text{sys,IRFs}}$	$\Delta_{\text{sys}}$
Energy flux ( $10^{-11}$ erg cm $^{-2}$ s $^{-1}$ )	4.69	0.38	+0.03/-0.73	+0.45/-0.36	+0.45/-0.81
$\Gamma_1$	0.89	0.29	+0.46/-1.00	+0.32/-1.37	+0.55/-1.70
$E_{\text{break}}$ (GeV)	1.72	0.40	+0.62/-0.17	+1.20/-0.87	+1.35/-0.89
$\Gamma_2$	2.17	0.09	+0.06/-0.02	+0.08/-0.05	+0.10/-0.05

Note. — Spectral fit of Cas A assuming a smoothly-broken power-law spectral model. Energy flux is quoted from 100 MeV to 100 GeV.  $\Delta_{\text{stat}}$  is the statistical error;  $\Delta_{\text{sys,diffuse}}$  is the estimated systematic error due to uncertainties in modeling the Galactic diffuse emission;  $\Delta_{\text{sys,IRFs}}$  is the estimated systematic error due to uncertainty in our knowledge of the IRFs of the LAT.  $\Delta_{\text{sys}}$  is derived by adding the two components of systematic errors in quadrature.



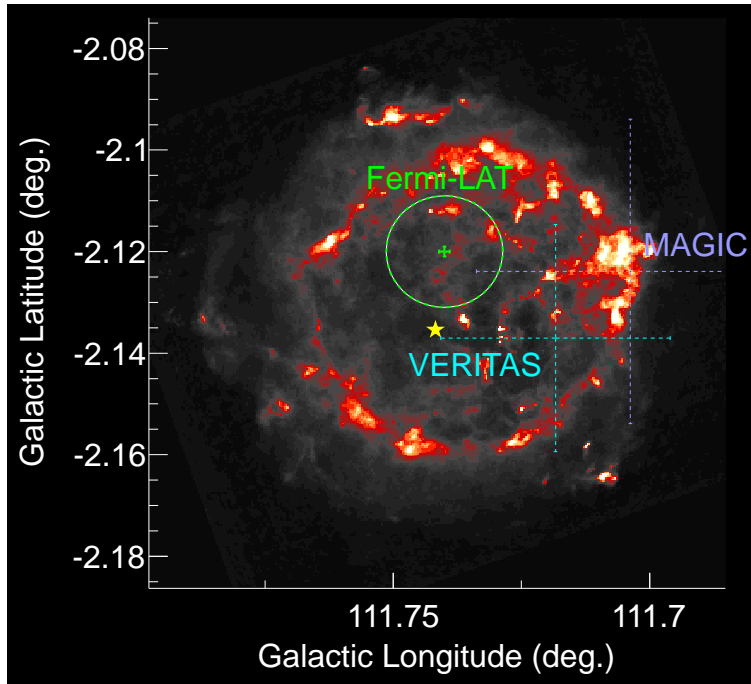


Fig. 2.— *Fermi*-LAT best-fit localization of Cas A (shown as a green cross, also shown is the error ellipse at 68% confidence level, calculated by adding statistical and systematic errors in quadrature), overlaid with VLA 20 cm radio map of the Cas A SNR (Anderson & Rudnick 1995). The central compact object is shown as a yellow star. Also shown are best-fit positions obtained by MAGIC (Albert et al. 2007) and VERITAS (Acciari et al. 2010).

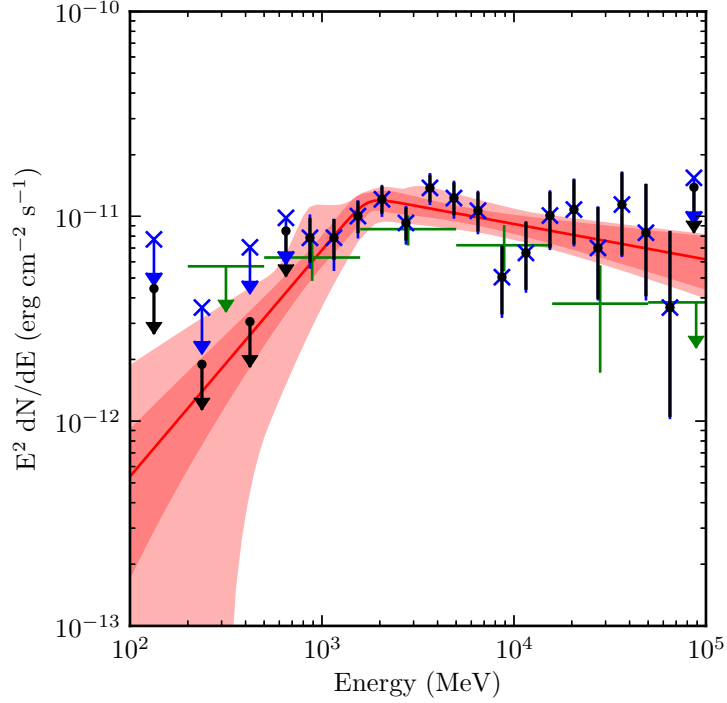


Fig. 3.— The spectral energy distribution of Cas A. The black points include statistical error only and the blue cross points include both statistical and systematic errors added in quadrature. The black upper limits consider only statistical effects and are calculated at 95% confidence level using a Bayesian method. We plot an upper limit instead of a data point when  $\text{TS} < 4$ . Blue upper limits have included systematic uncertainties. The red line is the best-fit spectral model assuming a smoothly-broken power law. The dark shaded region represents the statistical error on the spectral fit and the lightly shaded region represents the systematic and statistical errors added in quadrature. Also shown are the spectral points measured in Paper I (green points).

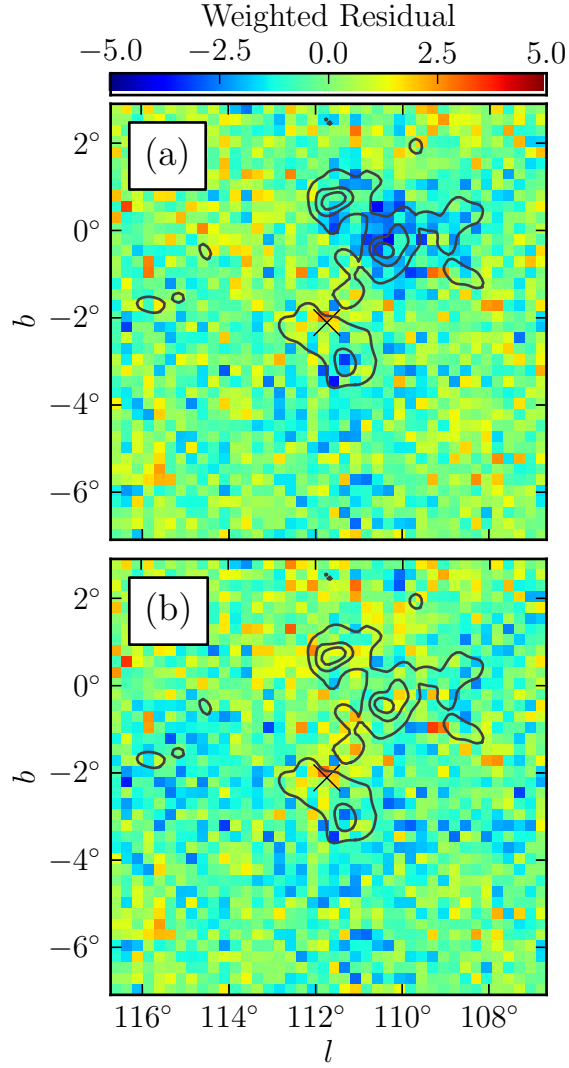


Fig. 4.— Weighted residual count maps (unsmoothed) in the energy range 100 MeV to 100 GeV after fitting with (a) standard diffuse model and (b) one of the alternative diffuse models. The weighted residual  $s$  is calculated as  $s = (N_{\text{obs}} - N_{\text{mdl}})/\sqrt{N_{\text{mdl}}}$ , where  $N_{\text{obs}}$  and  $N_{\text{mdl}}$  are observed count and model count, respectively. The location of Cas A is indicated by the black cross. The contours correspond to integrated intensity of the CO line and represent the column-density distribution of the molecular complex associated with NGC 7538 and Cas A (this is the same CO intensity map of the Perseus arm with the same velocity range of integration as described in Abdo et al. 2010b). The CO map was smoothed using a Gaussian kernel of  $0.5^\circ$ . Contours of 8, 29, and 50  $\text{K km s}^{-1}$  are shown.

174 updated background models. In Paper I, we argued that the GeV–TeV gamma rays detected  
 175 from Cas A can be interpreted in terms of either a leptonic or a hadronic model. In these  
 176 models, cosmic-ray electrons and protons (and ions) are accelerated in Cas A and produce  
 177 the gamma-ray emission. In what follows, we revisit the gamma-ray emission models and  
 178 then discuss the new LAT spectrum.

179 The synchrotron X-ray filaments found at the locations of outer shock waves indicate  
 180 efficient acceleration of cosmic-ray electrons at the forward shocks (Hughes et al. 2000;  
 181 Gotthelf et al. 2001; Vink & Laming 2003; Bamba et al. 2005; Patnaude & Fesen 2009).  
 182 Moreover, X-ray studies with *Chandra* suggest that electron acceleration to multi-TeV ener-  
 183 gies also takes place at the reverse shock propagating inside the supernova ejecta (Uchiyama & Aharonian  
 184 2008; Helder & Vink 2008). The detections of TeV gamma rays with HEGRA (Aharonian et al.  
 185 2001), MAGIC (Albert et al. 2007) and VERITAS (Acciari et al. 2010), established the ac-  
 186 celeration of multi-TeV particles in the remnant. Because of the small radius of 2.5′ of Cas A,  
 187 these experiments lacked the angular resolution to determine the spatial distribution of the  
 188 gamma rays and the sites of particle acceleration.

189 It is widely considered that diffusive shock acceleration (DSA: see e.g., Malkov & O’C Drury  
 190 2001, for a review) operating at the forward shocks is responsible for the energization  
 191 of the cosmic-ray particles. Most DSA models, which provide predictions of gamma-ray  
 192 spectra of SNRs, focus on the acceleration at the forward shock (e.g., Ellison et al. 2010;  
 193 Morlino & Caprioli 2012). Recently, newly-developed non-linear DSA models have included  
 194 the effects of acceleration of particles at reverse shocks and their subsequent transport  
 195 (Zirakashvili & Ptuskin 2012). Zirakashvili et al. (2013) have demonstrated that about 50%  
 196 of the gamma-ray flux at 1 TeV from Cas A can be contributed by the reverse-shocked  
 197 medium. Although the nonthermal X-ray filaments and knots in the reverse-shock region  
 198 are interesting sites of particle acceleration (Uchiyama & Aharonian 2008), we assume that  
 199 the gamma-ray emission comes predominantly from the forward shock region. Note that  
 200 our discussion on leptonic versus hadronic emission would not be greatly affected by this as-  
 201 sumption, because we allow for parameter space that is relevant also for the reverse-shocked  
 202 regions.

203 The gamma-ray emission models are constrained by the gas and radiation density and  
 204 by the magnetic field in the gamma-ray production region. We assume the simplest model  
 205 where cosmic rays are distributed uniformly in the shell of the remnant. The fluxes of  
 206 bremsstrahlung and  $\pi^0$ -decay gamma-ray emission scale linearly with the average gas density  
 207 ( $\propto \bar{n}$ ). Likewise the IC flux is proportional to the radiation energy density ( $\propto U_{\text{ph}}$ ) as long as  
 208 IC scattering is in the Thomson regime. The synchrotron flux scales as  $\propto B^{(s+1)/2}$  for a fixed  
 209 density of electrons with a power-law index of  $s$ . The magnetic field only indirectly affects

210 the gamma-ray flux by determining the amount of relativistic electrons that are required to  
 211 produce the observed synchrotron radio emission. This in turn can be used to calculate the  
 212 bremsstrahlung and IC fluxes. Therefore the gamma-ray flux constrains the magnetic field  
 213 in the shell (Cowsik & Sarkar 1980).

214 The outer shock waves are currently propagating into a dense circumstellar wind. The  
 215 density behind the blastwave is estimated as  $n_{\text{H}} \simeq 10 \text{ cm}^{-3}$  from the measured hydrodynam-  
 216 ical quantities such as shock velocities (Laming & Hwang 2003). The radiation field for IC  
 217 scattering is dominated by far infrared (FIR) emission from the shock-heated ejecta, char-  
 218 acterized by a temperature of 100 K and an energy density of  $\sim 2 \text{ eV cm}^{-3}$  (Mezger et al.  
 219 1986). Using the gas and infrared densities, which are well constrained from the multiwave-  
 220 length data, it was shown in Paper I that bremsstrahlung by relativistic electrons dominates  
 221 the leptonic component below  $\sim 1 \text{ GeV}$ , and IC/FIR becomes comparable to bremsstrahlung  
 222 above 10 GeV, for the assumed electron acceleration spectrum  $Q_e(E) \propto E^{-2.34} \exp(-E/E_m)$   
 223 with  $E_m = 40 \text{ TeV}$  (Vink & Laming 2003). The power-law index was set to match the  
 224 radio-infrared spectral index of  $\alpha = 0.67$  (Rho et al. 2003), since both the GeV gamma-ray  
 225 emission and the radio synchrotron emission sample similar electron energies. We note that  
 226 the IC scattering of FIR exceeds IC of cosmic microwave background by a factor of  $\sim 3$  at  
 227 10 GeV.

228 Figure 5 compares the leptonic model presented in Paper I with our new LAT mea-  
 229 surement. The magnetic field  $B = 0.1 \text{ mG}$  used in the leptonic model is consistent with  
 230  $B = 0.08\text{--}0.16 \text{ mG}$  estimated by Vink & Laming (2003) who interpreted the width of a syn-  
 231 chrotron X-ray filament as the synchrotron cooling length. The field is somewhat lower than  
 232  $B \simeq 0.3 \text{ mG}$  estimated by Parizot et al. (2006) who took into account a projection effect.  
 233 Unlike the TeV band where the electrons responsible for the gamma-ray emission suffer from  
 234 severe synchrotron losses, the gamma-ray spectral shape near 1 GeV does not depend on  
 235 the magnetic field. This can be seen, for example, in Araya & Cui (2010) who employed  
 236 different magnetic field strengths (by a factor of 6) between two radiation zones.

237 Also shown in Figure 5 is the hadronic model presented in Paper I. To achieve a  
 238 better match with the new measurement, the normalization of the model spectrum is in-  
 239 creased by 27% from Paper I. The model was calculated for a proton spectrum of  $Q_p(p) \propto$   
 240  $p^{-2.1} \exp(-p/p_m)$  with an exponential cutoff at  $cp_m = 10 \text{ TeV}$ , where  $p$  denotes momentum of  
 241 accelerated protons. The total proton content amounts to  $W_p(> 10 \text{ MeV } c^{-1}) \simeq 4 \times 10^{49} \text{ erg}$ ,  
 242 which is less than 2% of the estimated explosion kinetic energy of  $E_{\text{sn}} = 2 \times 10^{51} \text{ erg}$   
 243 (Laming & Hwang 2003; Hwang & Laming 2003)<sup>3</sup>.

---

<sup>3</sup> The shocked ejecta gas can contribute to the gamma-ray emission. The baryon density in the shocked

244 Paper I already showed that the leptonic model cannot fit the turnover well at low  
 245 energies because the bremsstrahlung component that is dominant over IC below 1 GeV has  
 246 a steep spectrum. Note that the spectral shape of the bremsstrahlung component copies  
 247 the electron spectrum with spectral index  $s = 2.34$ , which in turn is determined from the  
 248 radio-infrared spectral index of  $\alpha = 0.67$  (Rho et al. 2003). If we use a steeper power law  
 249 for the electron energy distribution based on a global spectral index of  $\alpha = 0.77$  in the  
 250 radio wavelengths (Baars et al. 1977) or a spectral shape with curvature that reproduces  
 251 the hardening ( $\alpha = 0.77 \rightarrow 0.67$ ) in the integrated spectrum, the discrepancies between the  
 252 bremsstrahlung model and the *Fermi*-LAT data become even larger. Araya & Cui (2010),  
 253 who reported the results of *Fermi*-LAT analysis of Cas A independently, also showed that the  
 254 electron bremsstrahlung with such a steep electron index could not explain the *Fermi*-LAT  
 255 spectrum. However, uncertainties in the Galactic diffuse emission at low energies prevented  
 256 a definitive conclusion regarding the inconsistency between the bremsstrahlung model and  
 257 the gamma-ray data. In this paper, a more detailed investigation of these uncertainties at  
 258 low energy now confirms the hadronic origin of the GeV  $\gamma$ -ray emission from Cas A. The  
 259 new LAT spectrum can be described by a broken power law with a second power-law index  
 260 of  $\Gamma_2 = 2.17 \pm 0.09$ . A comparison between the LAT spectrum and the TeV  $\gamma$ -ray spectra  
 261 suggests that additional steepening between the LAT and the TeV bands is necessary. Indeed,  
 262 the TeV  $\gamma$ -ray spectra measured with HEGRA, MAGIC, and VERITAS are consistent with  
 263 a power law with a photon index of  $\Gamma_{\text{TeV}} = 2.5 \pm 0.4_{\text{stat}} \pm 0.1_{\text{sys}}$ ,  $\Gamma_{\text{TeV}} = 2.3 \pm 0.2_{\text{stat}} \pm 0.2_{\text{sys}}$ ,  
 264 and  $\Gamma_{\text{TeV}} = 2.61 \pm 0.24_{\text{stat}} \pm 0.2_{\text{sys}}$ , respectively, which are somewhat steeper than the second  
 265 index  $\Gamma_2 = 2.17 \pm 0.09$  of the LAT spectrum. However, given the relatively large statistical  
 266 uncertainties of the TeV  $\gamma$ -ray fluxes, we refrain from solidifying the presence of the cutoff.  
 267 If confirmed, efficient acceleration of particles to PeV energies in Cas A is questioned.

268 The *Fermi*-LAT results on two historical SNRs, Tycho’s SNR (Giordano et al. 2012)  
 269 and Cas A, support hadronic scenarios for these objects. Tycho’s SNR is the remnant of a  
 270 Type Ia supernova, while Cas A is that of a core-collapse SN (specifically Type IIb). This in-  
 271 dicates that both Type Ia and core-collapse SNRs can convert a substantial fraction of their  
 272 kinetic expansion energies into cosmic-ray energies, and makes SNRs energetically favorable  
 273 candidates for the origin of Galactic cosmic rays. Recently, direct spectral signatures of  
 274 the  $\pi^0$ -decay emission have been found in two middle-aged SNRs interacting with molecular  
 275 clouds: W44 and IC 443 (Ackermann et al. 2013; Giuliani et al. 2011). Although spectro-  
 276 scopic evidence for the  $\pi^0$ -decay emission from Cas A is not as strong as these two cases, our

---

ejecta is similar to that in the forward shock region. Therefore, the total proton content estimated here  
 can be interpreted roughly as a sum of the cosmic-ray contents in the forward shock region and that in the  
 reverse-shocked ejecta.

277 results presented in this paper demonstrate the importance of the gamma-ray measurements  
 278 of SNRs below 1 GeV.

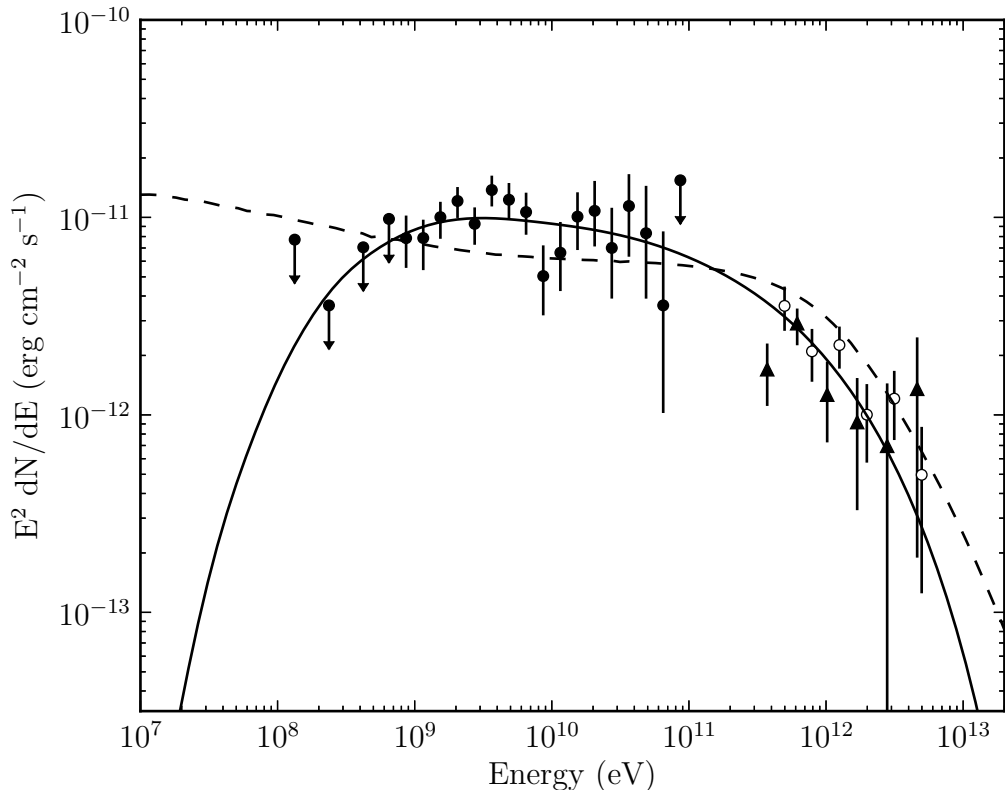


Fig. 5.— Gamma-ray spectrum of Cas A together with the emission models. The *Fermi*, MAGIC, and VERITAS points are plotted as filled circles, triangles and open circles, respectively (Albert et al. 2007; Acciari et al. 2010). The *Fermi* spectral points include both statistical and systematic errors. The curves show a leptonic model for  $B = 0.12$  mG (dashed line) and the hadronic model from Paper I with its normalization increased by 27% (solid line).

279 The *Fermi*-LAT Collaboration acknowledges generous ongoing support from a number  
 280 of agencies and institutes that have supported both the development and the operation of the  
 281 LAT as well as scientific data analysis. These include the National Aeronautics and Space  
 282 Administration and the Department of Energy in the United States, the Commissariat à  
 283 l’Energie Atomique and the Centre National de la Recherche Scientifique / Institut National  
 284 de Physique Nucléaire et de Physique des Particules in France, the Agenzia Spaziale Italiana  
 285 and the Istituto Nazionale di Fisica Nucleare in Italy, the Ministry of Education, Culture,



286 Sports, Science and Technology (MEXT), High Energy Accelerator Research Organization  
287 (KEK) and Japan Aerospace Exploration Agency (JAXA) in Japan, and the K. A. Wallen-  
288 berg Foundation, the Swedish Research Council and the Swedish National Space Board in  
289 Sweden.

290 Additional support for science analysis during the operations phase is gratefully acknowl-  
291 edged from the Istituto Nazionale di Astrofisica in Italy and the Centre National d'Études  
292 Spatiales in France.

## 293 REFERENCES

- 294 Abdo, A. A., et al. 2010a, *ApJ*, 710, L92  
295 —. 2010b, *ApJ*, 710, 133  
296 Acciari, V. A., et al. 2010, *ApJ*, 714, 163  
297 Ackermann, M., et al. 2012a, *ApJ*, 750, 3  
298 —. 2012b, *ApJS*, 203, 4  
299 —. 2013, *Science*, 339, 807  
300 Aharonian, F., et al. 2001, *A&A*, 370, 112  
301 Albert, J., et al. 2007, *A&A*, 474, 937  
302 Anderson, M. C., & Rudnick, L. 1995, *ApJ*, 441, 307  
303 Araya, M., & Cui, W. 2010, *ApJ*, 720, 20  
304 Atoyan, A. M., Tuffs, R. J., Aharonian, F. A., & Völk, H. J. 2000, *A&A*, 354, 915  
305 Atwood, W. B., et al. 2009, *ApJ*, 697, 1071  
306 Baars, J. W. M., Genzel, R., Pauliny-Toth, I. I. K., & Witzel, A. 1977, *A&A*, 61, 99  
307 Bamba, A., Yamazaki, R., Yoshida, T., Terasawa, T., & Koyama, K. 2005, *ApJ*, 621, 793  
308 Bykov, A. M., Uvarov, Y. A., & Ellison, D. C. 2008, *ApJ*, 689, L133  
309 Cowsik, R., & Sarkar, S. 1980, *MNRAS*, 191, 855

- 310 de Palma, F., Brandt, T. J., Johannesson, G., Tibaldo, L., & for the Fermi LAT collabora-  
311 tion. 2013, ArXiv e-prints
- 312 Ellison, D. C., Patnaude, D. J., Slane, P., & Raymond, J. 2010, *ApJ*, 712, 287
- 313 Giordano, F., et al. 2012, *ApJ*, 744, L2
- 314 Giuliani, A., et al. 2011, *ApJ*, 742, L30
- 315 Gotthelf, E. V., Koralesky, B., Rudnick, L., Jones, T. W., Hwang, U., & Petre, R. 2001,  
316 *ApJ*, 552, L39
- 317 Helder, E. A., & Vink, J. 2008, *ApJ*, 686, 1094
- 318 Helene, O. 1983, *Nuclear Instruments and Methods in Physics Research*, 212, 319
- 319 Hughes, J. P., Rakowski, C. E., Burrows, D. N., & Slane, P. O. 2000, *ApJ*, 528, L109
- 320 Hwang, U., & Laming, J. M. 2003, *ApJ*, 597, 362
- 321 Laming, J. M., & Hwang, U. 2003, *ApJ*, 597, 347
- 322 Lande, J., et al. 2012, *ApJ*, 756, 5
- 323 Maeda, Y., et al. 2009, *PASJ*, 61, 1217
- 324 Malkov, M. A., & O’C Drury, L. 2001, *Reports on Progress in Physics*, 64, 429
- 325 Mezger, P. G., Tuffs, R. J., Chini, R., Kreysa, E., & Gemuend, H.-P. 1986, *A&A*, 167, 145
- 326 Morlino, G., & Caprioli, D. 2012, *A&A*, 538, A81
- 327 Nolan, P. L., et al. 2012, *ApJS*, 199, 31
- 328 Parizot, E., Marcowith, A., Ballet, J., & Gallant, Y. A. 2006, *A&A*, 453, 387
- 329 Patnaude, D. J., & Fesen, R. A. 2007, *AJ*, 133, 147
- 330 —. 2009, *ApJ*, 697, 535
- 331 Pavlov, G. G., & Luna, G. J. M. 2009, *ApJ*, 703, 910
- 332 Reed, J. E., Hester, J. J., Fabian, A. C., & Winkler, P. F. 1995, *ApJ*, 440, 706
- 333 Rho, J., Reynolds, S. P., Reach, W. T., Jarrett, T. H., Allen, G. E., & Wilson, J. C. 2003,  
334 *ApJ*, 592, 299

- 335 Stecker, F. W. 1971, NASA Special Publication, 249
- 336 Uchiyama, Y., & Aharonian, F. A. 2008, ApJ, 677, L105
- 337 Vink, J., & Laming, J. M. 2003, ApJ, 584, 758
- 338 Zirakashvili, V. N., Aharonian, F. A., Yang, R., Ona-Wilhelmi, E., & Tuffs, R. J. 2013,  
339 ArXiv e-prints
- 340 Zirakashvili, V. N., & Ptuskin, V. S. 2012, Astroparticle Physics, 39, 12